ISSN 1674-1056
http://cpb.iphy.ac.cn
http://iopscience.iop.org/cpb
中国物理 B
Chinese Physics
中国物理
Chinese Physics B

Stationary response of stochastic viscoelastic system with the right unilateral nonzero offset barrier impacts

Deli Wang(王德莉), Wei Xu(徐伟), Xudong Gu(谷旭东)

Citation: Chin. Phys. B . 2019, 28(1): 010203. **doi:** 10.1088/1674-1056/28/1/010203
Journal homepage: http://cpb.iphy.ac.cn; http://iopscience.iop.org/cpb

What follows is a list of articles you may be interested in

Frequency response range of terahertz pulse coherent detection based on THz-induced time-resolved luminescence quenching

Man Zhang(张曼), Zhen-Gang Yang(杨振刚), Jin-Song Liu(刘劲松), Ke-Jia Wang(王可嘉), Jiao-Li Gong(龚姣丽), Sheng-Lie Wang(汪盛烈)

Chin. Phys. B . 2018, 27(6): 060204. **doi:** 10.1088/1674-1056/27/6/060204

Linear and nonlinear characteristics of time-resolved photoluminescence modulation by terahertz pulse

Jiao-Li Gong(龚姣丽), Jin-Song Liu(刘劲松), Man Zhang(张曼), Zheng Chu(褚政), Zhen-Gang Yang(杨振刚), Ke-Jia Wang(王可嘉), Jian-Quan Yao(姚建铨)

Chin. Phys. B . 2017, 26(10): 100201. **doi:** 10.1088/1674-1056/26/10/100201

Nonlinear radiation response of n-doped indium antimonide and indium arsenide in intense terahertz field

Jiao-Li Gong(龚姣丽), Jin-Song Liu(刘劲松), Zheng Chu(褚政), Zhen-Gang Yang(杨振刚), Ke-Jia Wang(王可嘉), Jian-Quan Yao(姚建铨)

Chin. Phys. B . 2016, 25(10): 100203. **doi:** 10.1088/1674-1056/25/10/100203

Improved locality-sensitive hashing method for the approximate nearest neighbor problem

Lu Ying-Hua, Ma Ting-Huai, Zhong Shui-Ming, Cao Jie, Wang Xin, Abdullah Al-Dhelaan

Chin. Phys. B . 2014, 23(8): 080203. **doi:** 10.1088/1674-1056/23/8/080203

Stationary response of stochastic viscoelastic system with the right unilateral nonzero offset barrier impacts*

Deli Wang(王德莉)[1], Wei Xu(徐伟)[1,†], and Xudong Gu(谷旭东)[2]

[1] Department of Applied Mathematics, Northwestern Polytechnical University, Xi'an 710072, China
[2] Department of Engineering Mechanics, Northwestern Polytechnical University, Xi'an 710072, China

(Received 29 June 2018; revised manuscript received 13 November 2018; published online 27 December 2018)

The stationary response of viscoelastic dynamical system with the right unilateral nonzero offset barrier impacts subjected to stochastic excitations is investigated. First, the viscoelastic force is approximately treated as equivalent terms associated with effects. Then, the free vibro-impact (VI) system is absorbed to describe the periodic motion without impacts and quasi-periodic motion with impacts based upon the level of system energy. The stochastic averaging of energy envelope (SAEE) is adopted to seek the stationary probability density functions (PDFs). The detailed theoretical results for Van der Pol viscoelastic VI system with the right unilateral nonzero offset barrier are solved to demonstrate the important effects of the viscoelastic damping and nonzero rigid barrier impacts condition. Monte Carlo (MC) simulation is also performed to verify the reliability of the suggested approach. The stochastic P-bifurcation caused by certain system parameters is further explored. The variation of elastic modulus from negative to zero and then to positive witnesses the evolution process of stochastic P-bifurcation. From the vicinity of the common value to a wider range, the relaxation time induces the stochastic P-bifurcation in the two interval schemes.

Keywords: viscoelastic system, right unilateral nonzero offset barrier impacts, stochastic averaging of energy envelope (SAEE), stochastic P-bifurcation

PACS: 02.50.Cw, 02.50.Ng, 05.10.Gg, 05.40.Ca **DOI:** 10.1088/1674-1056/28/1/010203

1. Introduction

Viscoelastic materials, such as polymer (viscoelastic anti-corrosion adhesive tape), synthetic material (synthetic rubber and geomembrane), and metallurgical material (brake pad and loose-hole sheet), with the advantages of anti-corrosion,[1] shock absorption, and noise reduction,[2,3] are favored in practical applications from life and production to construction engineering, aerospace, medical science, and other fields. Thus, viscoelastic property has attracted a lot of attention in scientific research. For viscoelastic materials, the stress depends on the history of strain, which is different from the classical elasticity.[4] It could be designed as a damping layer where the characteristic depends on frequency and temperature.[5] It has been observed that the strain of a viscoelastic material under constant stress increases with time in creep tests, while the stress decreases with time under constant strain in relaxation tests.[6] Based on such consideration, a generalized Maxwell model[7,8] has been developed to describe the relaxation function.

In the previous literature, the nonlinear dynamic study of viscoelastic systems has mainly focused on the deterministic case.[9–11] Due to the widespread existence of random perturbations in practical applications,[12–14] it is quite significant to investigate the behavior of viscoelastic systems under stochastic excitations. Potapov[15] analyzed the stability of stochastic viscoelastic systems by the method of stochastic averaging. Cai and Zhu[16] improved the stochastic averaging method based on the viscoelastic system. Huang *et al.*[17] studied the stability of a single-degree-of-freedom (SDOF) linear viscoelastic system by using both first-order and second-order stochastic averaging methods. Mario and collaborators[18] considered stationary and non-stationary stochastic response of linear fractional viscoelastic systems. Christian and Poloskov[19] provided time-domain formulation in computational dynamics for linear viscoelastic media with model uncertainties and stochastic excitation.

In addition, a number of non-smooth factors[20] exist in engineering applications; for instance, the interactions of a mechanical or structural system with a rigid obstacle will result in a non-smooth effect, which is modeled as impact. The interaction of the system with obstacles can be either elastic or inelastic.[21] Thus, the dynamics of vibro-impact (VI) systems has been further studied.[22–28] Zhuralev has introduced a non-smooth transformation to study the VI system with rigid barriers,[29] and Wu and Zhu extended this method to multiple-degrees-of-freedom (MDOF) VI systems under Poisson white noise excitations;[30] some further developments of this method have been made subsequently.[31–33] Chattering bifurcations were considered in a Duffing unilateral VI system.[34] The finite element method and a measure based

*Project supported by the National Natural Science Foundation of China (Grant Nos. 11872305 and 11872307) and the Excellent Doctorate Cultivating Foundation of Northwestern Polytechnical University, China.

†Corresponding author. E-mail: weixu@nwpu.edu.cn

© 2019 Chinese Physical Society and IOP Publishing Ltd

on the Shannon entropy[35–37] were described in a noisy VI Duffing–Van der Pol oscillator. Resonance response of a nonlinear VI system to a narrow-band random parametric excitation are analyzed in Ref. [38]. In addition, the studies on stochastic bifurcation in Refs. [39]–[44] are referenced. Most of the previous studies have concentrated on the responses of linear VI systems with zero rigid barrier or nonlinear smooth systems, and only a few considered the responses of nonlinear nonzero offset barrier impacts oscillator coupled with the viscoelastic force.

This paper mainly focuses on the stationary response considerations of the stochastic viscoelastic system with right nonzero offset barrier impacts. The structure of the paper is as follows. The original system and viscoelastic damping treatment are described in Section 2. In Section 3, the free VI system is analyzed, and then the approximate stationary probability density functions (PDFs) are derived by the stochastic averaging approach of energy envelope. An example of Van der Pol viscoelastic VI oscillator with the right nonzero rigid barrier is carried out and the analytical solutions observed from the suggested method are well tested by the results from the Monte Carlo (MC) simulation in Section 4.1, and the stochastic P-bifurcation caused by certain parameters is explored in Section 4.2. The conclusion is summarized in the last section.

2. Problem statement

2.1. Original system description

An SDOF lightly damped viscoelastic system with right unilateral nonzero offset barrier impacts behavior under random excitations is investigated, which is schematically shown in Fig. 1. The equation of the system is of the form

$$\ddot{x}+\varepsilon d(x,\dot{x})+\varepsilon V+r(x)=\varepsilon^{1/2}l_m(x,\dot{x})\eta_m(t),\quad x<S_0, \tag{1a}$$

$$\dot{x}_+=-\rho\dot{x}_-,\quad x=S_0. \tag{1b}$$

In Eq. (1a), ε is a small positive parameter, and the dot indicates differentiation with respect to time; $\varepsilon d(x,\dot{x})$ represents lightly linear or nonlinear damping force; $r(x)$ denotes the nonlinear or linear restoring force as an odd function of x; $\eta_m(t)$ represents Gaussian white noises in the sense of Stratonovich, and possesses correlation functions $E[\eta_n(t)\eta_k(t+\tau_0)]=2D_{nk}\delta(\tau_0)$; and $\varepsilon^{1/2}l_m(x,\dot{x})$ $(m\in N^+)$ describes amplitudes of weakly random perturbations. Equation (1b) is the impact condition for the inelastic instantaneous interaction, where ρ in $[0,1]$ is a restitution factor. $\dot{x}_-$ and $\dot{x}_+$ represent the velocity of the system before and after the instant of impacts; S_0 denotes the position of the nonzero rigid barrier.

The constitutive model of viscoelastic damping is provided as[11]

$$V[x(t)]=\int_0^t q(t-\mu)x(\mu)\mathrm{d}\mu, \tag{2}$$

and the relaxation function $q(t)$ is expressed as follows based on Refs. [9] and [11]:

$$q(t)=\sum_i \beta_i\exp(-t/\lambda_i),\quad \lambda_i\geq 0. \tag{3}$$

Each λ_i in Eq. (3) is the relaxation time of the viscoelastic components, and β_i specifies elastic modulus being either positive or negative. Both parameters are determined by the concrete problems.

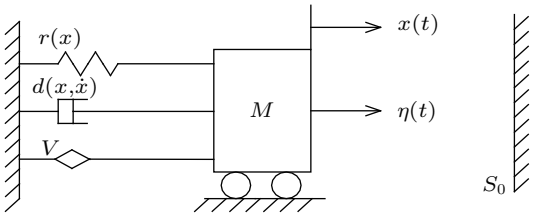


Fig. 1. Schematic model of the viscoelastic oscillator with right unilateral nonzero offset barrier impacts.

2.2. Treatment for the viscoelastic force

Taking into account that the viscoelastic force contributes to both the stiffness and the damping,[16] system equations (1a) and (1b) can be written as

$$\ddot{x}+\varepsilon d_1(x,\dot{x})+r_1(x)=\varepsilon^{1/2}l_m(x,\dot{x})\eta_m(t),\quad x<S_0, \tag{4a}$$

$$\dot{x}_+=-\rho\dot{x}_-,\quad x=S_0. \tag{4b}$$

Here, the consideration of the viscoelastic force has been incorporated in $d_1(x,\dot{x})$ and $r_1(x)$, respectively. The potential energy function $U(x)$ and the total energy E of the system are

$$U(x)=\int_0^x r_1(\upsilon)\mathrm{d}\upsilon, \tag{5}$$

$$E=\dot{x}^2/2+U(x). \tag{6}$$

The period of the corresponding free motion is given by

$$T=\oint[2E-2U(x)]^{-1/2}\mathrm{d}x=4\int_0^A[2E-2U(x)]^{-1/2}\mathrm{d}x, \tag{7}$$

where A is the amplitude for a given E, and the positive root is calculated from $E=U(A)$.

The motion equations of the system (4a) and (4b) can be described through variable substitution. Utilize the total energy $E(t)$ and the total phase angle $\vartheta(t)$ according to the transformation

$$\begin{aligned}&\mathrm{sgn}x\,[U(x)]^{1/2}=\sqrt{E}\cos\vartheta(t),\\&\dot{x}=-\sqrt{2E}\sin\vartheta(t),\end{aligned} \tag{8}$$

and $\vartheta(t)$ is defined as

$$\begin{aligned}&\vartheta(t)=\int_0^t\omega(\nu)\mathrm{d}\nu+\phi(t),\\&\omega(t)=r_1(x)\left(\sqrt{2E}\cos\vartheta\right)^{-1}.\end{aligned} \tag{9}$$

$\phi(t)$ denotes the residue phase angle, and $\omega(t)$ is the instantaneous frequency. The average frequency of $\omega(t)$ can be calculated by the quasi-period T

$$\bar{\omega} = \frac{2\pi}{T}. \tag{10}$$

Denote each component in the viscoelastic force exhibited in Eqs. (2) and (3) as

$$V_i = \int_0^t \beta_i \mathrm{e}^{-(t-\upsilon)/\lambda_i} x(\upsilon)\mathrm{d}\upsilon. \tag{11}$$

Applying the transformation of Eq. (8) with $\vartheta(t) \approx \bar{\omega}t + \phi$, and neglecting the decaying transient part, we can get

$$V_i = \beta_i\lambda_i \left(1+\bar{\omega}^2\lambda_i^2\right)^{-1}(-\lambda_i\dot{x}+x). \tag{12}$$

Thus, functions $d_1(x,\dot{x})$ and $r_1(x)$ in Eq. (4a) are derived by Eq. (12) as

$$\begin{aligned} d_1(x,\dot{x}) &= d(x,\dot{x}) - \sum_i \left[\beta_i\lambda_i^2\left(1+\bar{\omega}^2\lambda_i^2\right)^{-1}\dot{x}\right], \\ r_1(x) &= r(x) + \sum_i \left[\beta_i\lambda_i\left(1+\bar{\omega}^2\lambda_i^2\right)^{-1}x\right]. \end{aligned} \tag{13}$$

Besides, combining Eqs. (7) and (10), the average frequency $\bar{\omega}$ is determined

$$\frac{\pi}{\bar{\omega}} = 2\int_0^A [2E-2U(x)]^{-1/2}\mathrm{d}x. \tag{14}$$

Thus, viscoelastic system equations (1a) and (1b) with unilateral nonzero offset barrier impacts are transformed to the system Eqs. (4a) and (4b) without viscoelastic damping form.

3. Stochastic averaging approach

3.1. Free VI system analysis

Introducing $\dot{x} = y$, equation (4a) can be rewritten as the following Itô stochastic differential equations:

$$\begin{aligned} &\mathrm{d}x = y\mathrm{d}t, \\ &\mathrm{d}y = \Gamma(x,y)\mathrm{d}t + \Sigma(x,y)\mathrm{d}W(t), \quad x < S_0, \end{aligned} \tag{15}$$

where $\Gamma(x,y)$ and $\Sigma(x,y)$ denote drift and diffusion representations, and $W(t)$ is a unit Weiner process.

The potential energy function and total energy of the system have been reported in the previous Eqs. (5) and (6), respectively. When the parameter ε is zero, equations (15) and (4b) constitute a free VI system. Suppose functions $r_1(x)$ and $U(x)$ are such that the free VI system associated with Eq. (15) without impact has a gens periodic solutions surrounding the origin on phase plane (x,y). The period is the same as earlier

$$T(E) = 2\int_{-a}^{a}\left[\sqrt{2E-2U(x)}\right]^{-1}\mathrm{d}x. \tag{16}$$

Here, a denotes the maximum displacement derived by $E = U(a)$. As $E > U(S_0)$, the system will impact the nonzero offset barrier. The system state before impact is $\dot{x} = \dot{x}_-$, and the system energy can be written as

$$E_- = \dot{x}_-^2/2 + U(S_0). \tag{17}$$

When the impact occurs, the system state after impact with the nonzero offset barrier turns into $\dot{x} = \dot{x}_+ = -\rho\dot{x}_-$, and the system energy becomes

$$E_+ = \dot{x}_+^2/2 + U(S_0). \tag{18}$$

The loss of the system energy during each impact is calculated as

$$\Delta E = E_- - E_+ = (1-\rho^2)\left[E_- - U(S_0)\right]. \tag{19}$$

The system still moves as a free oscillator between the first impact $(t = t_1)$ and the second impact $(t = t_2)$, and the time period Δt of the process between both consecutive impacts can be evaluated by

$$\Delta t = t_2 - t_1 = 2\int_{-a}^{S_0}\left[\sqrt{2E-2U(x)}\right]^{-1}\mathrm{d}x. \tag{20}$$

The time period can be seen as the period of free oscillation after occurrence of impacts, which relies on the system energy; thus, denoted as $T(E) = \Delta t$ represents the quasi-period. It is implied from Eq. (19) that the energy loss ΔE is related to the restitution factor ρ, the energy before nonzero rigid barrier impacts, the nonzero position S_0, and the viscoelastic force due to its equivalent stiffness part.

3.2. Stochastic averaging of energy envelope (SAEE)

Relying on the Eqs. (6) and (15), the Itô equations for displacement x and system energy E can be derived by employing the Itô differential rule. When the damping, the stochastic excitation, and the energy loss are small, it can be found that energy $E(t)$ is a slowly varying process, and the displacement $x(t)$ is a rapidly varying process. Thus, the method of SAEE[45] is absorbed here. Further, the averaged Itô equation for $E(t)$ is given as

$$\mathrm{d}E = \Gamma(E)\mathrm{d}t + \Sigma(E)\mathrm{d}B(t), \tag{21}$$

where $\Gamma(E)$ and $\Sigma(E)$ are averaged drift and diffusion representations, and $B(t)$ is the standard Brownian motion process.

For the situation of $E < U(S_0)$, the system keeps the vibration without impact. The drift and diffusion representations of the viscoelastic system with nonzero offset barrier impacts remain as

$$\begin{aligned} \Gamma(E) &= [T(E)]^{-1}\int_{-A}^{A}\{-2\varepsilon d_1(x,[2E-2U(x)]^{1/2}) \\ &\quad + [2E-2U(x)]^{-1/2}\Sigma^2(x,[2E-2U(x)]^{1/2})\}\mathrm{d}x, \end{aligned} \tag{22a}$$

$$\Sigma^2(E) = [T(E)]^{-1}\int_{-A}^{A}\{[2E-2U(x)]^{1/2}$$

$$\times 2\Sigma^2(x,[2E-2U(x)]^{1/2})\}\mathrm{d}x, \tag{22b}$$

$$T(E) = \int_{-A}^{A} 2\left[2E-2U(x)\right]^{-1/2}\mathrm{d}x. \tag{22c}$$

As E exceeds $U(S_0)$, the system possesses the vibration with the impact. The energy loss during impact needs to be counted; thus, the averaged drift and diffusion representation becomes

$$\begin{aligned}\Gamma(E) &= [T(E)]^{-1}\int_{-A}^{S_0}\{-2\varepsilon d_1(x,[2E-2U(x)]^{1/2}) \\ &\quad + [2E-2U(x)]^{-1/2}\Sigma^2(x,[2E-2U(x)]^{1/2})\}\mathrm{d}x \\ &\quad - \Delta E\,[T(E)]^{-1}, \end{aligned}\tag{23a}$$

$$\begin{aligned}\Sigma^2(E) &= [T(E)]^{-1}\int_{-A}^{S_0}\{[2E-2U(x)]^{1/2} \\ &\quad \times 2\Sigma^2(x,[2E-2U(x)]^{1/2})\}\mathrm{d}x, \end{aligned}\tag{23b}$$

$$T(E) = \int_{-A}^{S_0} 2\left[2E-2U(x)\right]^{-1/2}\mathrm{d}x, \tag{23c}$$

where $A = U^{-1}(E)$ denotes the amplitude of vibration, and $\Delta E\,[T(E)]^{-1}$ describes the energy loss during each impact.

Further, the averaged Fokker–Plank–Kolmogorov (FPK) equation associated with Itô Eq. (21) is expressed as

$$\frac{\partial p}{\partial t} = \frac{\partial^2[\Sigma^2(E)p/2]}{\partial E^2} - \frac{\partial\left[\Gamma(E)p\right]}{\partial E}, \tag{24}$$

where $p = p(E,t|E_0)$ represents the transition probability density of E dependent on the initial condition

$$p(E,0|E_0) = \delta(E-E_0), \tag{25}$$

and the boundary condition is finite for the situation of $E=0$, while

$$p, \frac{dp}{dE} \to 0, \quad E\to\infty. \tag{26}$$

Thus, the stationary solution of Eq. (24) can be provided by

$$p(E) = Z\Sigma^{-2}(E)\exp\left\{\int_0^E\left[2\Gamma(\upsilon)\Sigma^{-2}(\upsilon)\right]\mathrm{d}\upsilon\right\}, \tag{27}$$

where Z is the normalization constant.

Next, the joint probability density of the displacement and the velocity can be calculated

$$p(x,y) = p(x,E)\left|\begin{array}{cc}\partial x/\partial x & \partial x/\partial y \\ \partial E/\partial x & \partial E/\partial y\end{array}\right| = |y|\,p(x|E)p(E). \tag{28}$$

Here, $p(x|E)$ is the conditional probability density function, which can be given by

$$p(x|E) = Z'|y|^{-1} = Z'\left[2E-2U(x)\right]^{-1/2}. \tag{29}$$

The normalization constant Z' is computed by

$$Z' = \left\{\oint\left[2E-2U(x)\right]^{-1/2}\mathrm{d}x\right\}^{-1} = T^{-1}. \tag{30}$$

Substituting Eqs. (29) and (30) into Eq. (28) yields

$$p(x,y) = p(E)\left[T(E)\right]^{-1}\Big|_{E=y^2/2+U(x),\ x\le S_0}. \tag{31}$$

Then, the marginal probability density functions $p(x)$ and $p(y)$ can be solved by

$$p(x) = \int_{-\infty}^{\infty} p(x,\zeta)\mathrm{d}\zeta, \tag{32a}$$

$$p(y) = \int_{-\infty}^{S_0} p(\upsilon,y)\mathrm{d}\upsilon. \tag{32b}$$

4. Application and simulation

Here, we adopt the nonlinear viscoelastic oscillator with right nonzero rigid barrier impacts to illustrate the analytical procedure

$$\begin{aligned}&\ddot{x}+\hat{d}(x,\dot{x})+V'+\sigma x = \eta(t),\ \ x<S_0,\\ &V' = \beta_1\int_0^t \mathrm{e}^{-(t-s)/\lambda_1}x(s)\mathrm{d}s,\\ &\dot{x}_+ = -\rho\dot{x}_-,\ \ x=S_0.\end{aligned}\tag{33}$$

The damping force $\hat{d}(x,\dot{x})$ and viscoelastic force V' here are assumed to be of order ε, and $\eta(t)$ are stationary broad-band random processes of order $\varepsilon^{1/2}$, i.e., the Gaussian white noise with intensity $2D'$. σ denotes the nature frequency. ρ and S_0 are described the same as the previous interpretation. By approximating V' based on Eqs. (12) and (13) to the case, the equivalent system of Eq. (33) has the form

$$\begin{aligned}&\ddot{x}+\hat{d}_1(x,\dot{x})+\hat{r}_1(x) = \eta(t),\ \ x<S_0,\\ &\dot{x}_+ = -\rho\dot{x}_-,\ \ x=S_0,\end{aligned}\tag{34}$$

where $\hat{d}_1(x,\dot{x}) = \hat{d}(x,\dot{x}) - \left[\beta_1\lambda_1^2\left(1+\bar{\omega}^2\lambda_1^2\right)^{-1}\right]\dot{x}$ and $\hat{r}_1(x) = \left[\sigma+\lambda_1\beta_1\left(1+\bar{\omega}^2\lambda_1^2\right)^{-1}\right]x$.

According to Eq. (14), specifically for the present case, the average frequency $\bar{\omega}$ can be given by

$$\bar{\omega}^2 = \left(2\lambda_1^2\right)^{-1}\left\{\lambda_1^2\sigma+\left[(1+\lambda_1^2\sigma)^2+4\beta_1\lambda_1^3\right]^{1/2}-1\right\}. \tag{35}$$

Relying on the method of SAEE, the drift and diffusion representations of the averaged Itô equation for energy E can be obtained in detail.

For the situation of $E<U(S_0)$, combining with Eqs. (22a)–(22c), let $f = \sigma+\lambda_1\beta_1\left(1+\bar{\omega}^2\lambda_1^2\right)^{-1}$, and then yield

$$\begin{aligned}&\Gamma(E) = D' - [T(E)]^{-1}\int_{-A}^{A}2\hat{d}_1(x,\left(2E-fx^2\right)^{1/2})\mathrm{d}x,\\ &A = (2E/f)^{1/2},\\ &T(E) = \int_{-A}^{A}2\left(2E-fx^2\right)^{-1/2}\mathrm{d}x = \frac{4}{\sqrt{f}}\arcsin\left(A\sqrt{\frac{f}{2E}}\right),\\ &\Sigma^2(E) = [T(E)]^{-1}\int_{-A}^{A}4D'\left(2E-fx^2\right)^{1/2}\mathrm{d}x\\ &\qquad = 2D'E + 2D'AE\sqrt{\frac{f}{2E}}\sqrt{1-\frac{fA^2}{2E}}\end{aligned}$$

$$\times \left[\arcsin\left(A\sqrt{\frac{f}{2E}}\right)\right]^{-1}. \tag{36}$$

As E exceeds $U(S_0)$, combining with Eqs. (23a)–(23c), we can get

$$\begin{aligned}
\Gamma(E) &= D' - [T(E)]^{-1} \\
&\quad \times \left\{\int_{-A}^{S_0} 2\hat{d}_1(x,(2E-fx^2)^{1/2})\mathrm{d}x - \Delta E\right\}, \\
\Delta E &= (1-\rho^2)\left[E - fS_0^2/2\right], \\
\Sigma^2(E) &= [T(E)]^{-1}\int_{-A}^{S_0} 4D'\left(2E-fx^2\right)^{1/2}\mathrm{d}x \\
&= 2D'E + 2D'E\left(S_0\sqrt{\frac{f}{2E}}\sqrt{1-\frac{fS_0^2}{2E}}\right. \\
&\quad \left. + A\sqrt{\frac{f}{2E}}\sqrt{1-\frac{fA^2}{2E}}\right) \\
&\quad \times \left[\arcsin\left(S_0\sqrt{\frac{f}{2E}}\right) + \arcsin\left(A\sqrt{\frac{f}{2E}}\right)\right]^{-1}, \\
T(E) &= \int_{-A}^{S_0} 2\left(2E-fx^2\right)^{-1/2}\mathrm{d}x \\
&= \frac{2}{\sqrt{f}}\left[\arcsin\left(S_0\sqrt{\frac{f}{2E}}\right) + \arcsin\left(A\sqrt{\frac{f}{2E}}\right)\right].
\end{aligned} \tag{37}$$

Next, by solving the averaged FPK Eq. (24), we obtain the PDFs of the system energy E, and further get the probability density functions $p(x,y)$, $p(x)$, and $p(y)$ based on Eqs. (31), (32a), and (32b). And then consider the case of $\hat{d} = \left[d_0\dot{x} - d_2x^2\dot{x}\right]$, system equation (33) represents a nonlinearly damped and stochastically excited Van der Pol viscoelastic VI system.

4.1. Validity of the approach

The analytical stationary PDFs will be exhibited and compared with the directly numerical simulation results. All the directly numerical simulations computed by employing the Runge–Kutta (RK) algorithm and Monte Carlo method are presented based on the original system Eq. (33), which provide the validation as well as rationality of the analytic results. Solutions are initially observed with the parameters: $d_0 = -0.01$, $d_2 = -0.005$, $\sigma = 1.0$, $\beta_1 = -0.2$, $\lambda_1 = 1.1$, $\rho = 0.9$, $S_0 = 0.995$, and $D' = 0.0236$, unless otherwise stated. Then, the effects on the system responses for the intensity D' of stochastic process $\eta(t)$, two viscoelastic parameters β_1 and λ_1, the position S_0 of the right nonzero rigid barrier, and the restitution factor are described in detail in Figs. 2–5. The increase of noise intensity D', i.e., gaining stronger external force leads to lower peaks of stationary PDFs of the displacement x and the velocity y, and smaller values for the stationary PDFs of total energy E at small energy, i.e., make ones more flat in Figs. 2(a)–2(c) and the oscillator stays at equilibrium with a smaller possibility. Besides, figure 2(a) shows that the increase of D' can contribute to the system with high energy, large displacement, and velocity, i.e., obtaining larger probability of the system. It can be seen that the approximate analytical results are relatively close to the directly numerical ones.

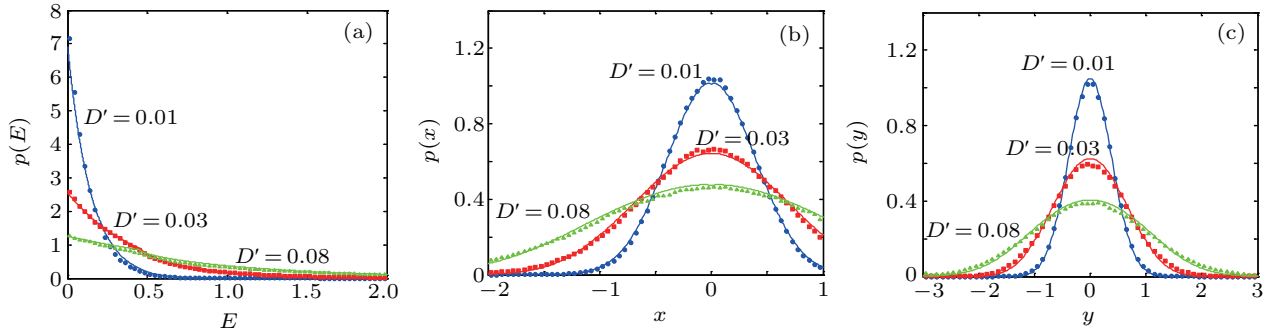


Fig. 2. Stationary PDFs of (a) total energy E, (b) displacement x, and (c) velocity y, solved both analytically and numerically with different noise intensities. Solid lines represent analytical results, while circles, squares, and triangles represent Monte Carlo simulation results.

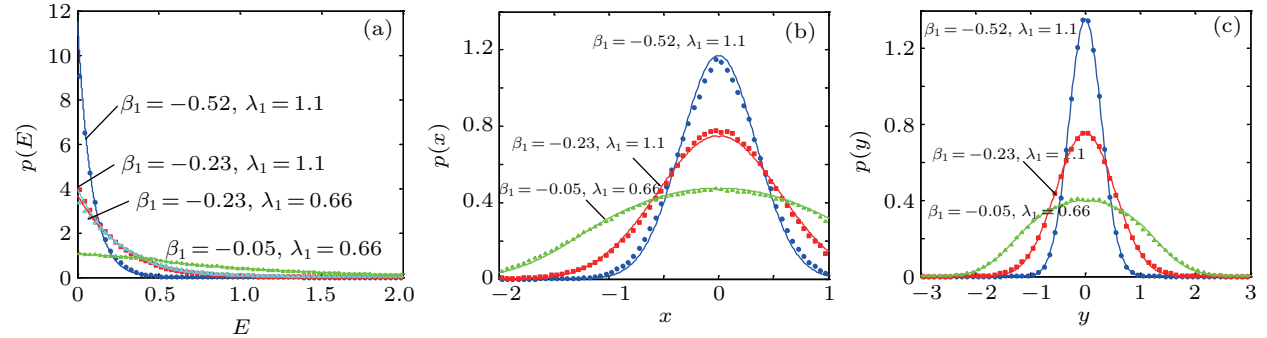


Fig. 3. Stationary PDFs of (a) total energy E, (b) displacement x, and (c) velocity y, solved both analytically and numerically with different viscoelastic parameters. Solid lines represent analytical results, while circles, squares, and triangles represent Monte Carlo simulation results.

The elastic modulus β_1 and relaxation time λ_1 show a difference in responses of the system according to Fig. 3. β_1 keeps negative in Fig. 3, and the change of stationary PDFs caused by the variation of $|\beta_1|$ is stronger than that caused by the variation of λ_1. The increase in $|\beta_1|$ is equivalent to an increase in the damping effect, which can contribute to higher peaks of stationary PDFs of displacement and velocity, and larger values for the stationary PDFs of total energy E at small energy, indicating a larger probability that the system will stay close to the equilibrium state. The two solutions here also agree well.

Examination of the position S_0 of the right nonzero rigid barrier and the restitution factor ρ on the system response are illustrated in Figs. 4 and 5, respectively. Curves in Fig. 4(a) show unsmoothness at $E = U(S_0)$. When the oscillator is further away from the obstacle position in Figs. 4(b) and 4(c), which is equivalent to reducing the damping effect, it leads to lower peaks of stationary PDFs of displacement and velocity, and smaller values for the stationary PDFs of total energy E at small energy, indicating a smaller probability that the system will stay close to the equilibrium state. Additionally, when S_0 reaches the amplitude of the oscillator motion, i.e., the maximum displacement which is approximately 1.995 here, the corresponding response probability is close to 0, indicating that if S_0 crosses the threshold, the impacts will not occur. In Figs. 5(a)–5(c), the variation of restitution factor ρ from 0.45 to 0.94 does not cause a great change in the response probability of the system. It can be found that the analytical results and MC simulation results agree well in these figures, which further indicates that the analytical procedure is reliable and effective via the related comparisons.

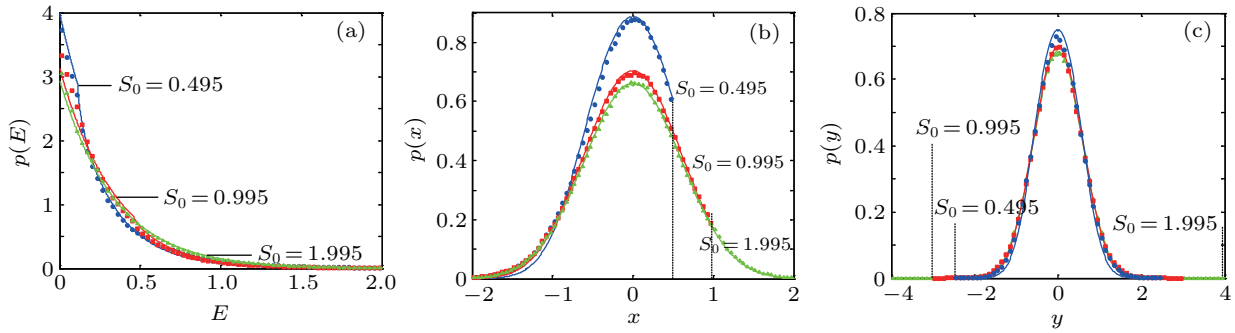


Fig. 4. Stationary PDFs of (a) total energy E, (b) displacement x, and (c) velocity y, solved both analytically and numerically with different positions of the nonzero rigid barrier. Solid lines represent analytical results, while circles, squares, and triangles represent Monte Carlo simulation results.

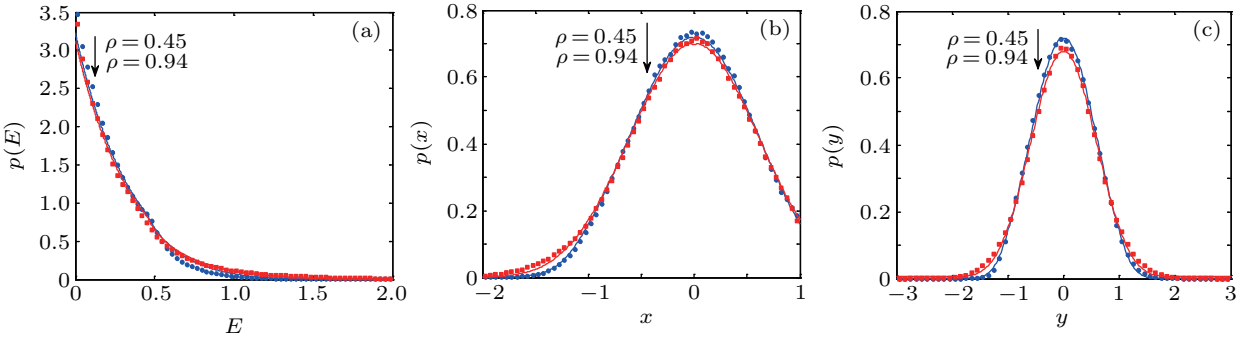


Fig. 5. Stationary PDFs of total energy (a) E, (b) displacement x, and (c) velocity y, solved both analytically and numerically with different restitution factor values. Solid lines represent analytical results, while circles and squares represent Monte Carlo simulation results.

4.2. Further analysis: stochastic P-bifurcations

According to Section 4.1, satisfactory agreement is shown between the results of analytical procedure and MC simulation solution obtained from the original stochastic VI system. Based upon the above conclusion, a further analysis for joint stationary PDFs of the displacement x and the velocity y is observed here, and stochastic P-bifurcation occurs with the variation of certain parameters. Thus, we perform the exploration for stochastic P-bifurcation in this subsection. Take $\rho = 0.95$ and $S_0 = 0.985$, and the rest are kept the same as the initial values.

The position S_0 of the nonzero rigid barrier varies from 0.985 in Figs. 6(a), 6(b), and 6(d) to 1.985 in Fig. 6(c), and the figures exhibit the decreasing joint PDFs and the corresponding analytical and numerical contour lines for different elastic moduli β_1 being negative, which is the response to the result in Fig. 3. The contours of the two solutions further change from Fig. 7(a) to Fig. 7(d) with the large-amplitude oscillations and the small-amplitude oscillations around the origin at the position of $S_0 = 0.485$ when some parameters are in the bifurcation

schemes, and the phenomenon here will be discussed below. Besides, the analytical solutions and MC simulation ones on the contours of joint PDFs agree well here, which responds to the previous conclusion.

Next, figures 8, 10, 12, and 14(a)–14(c) provide joint stationary PDFs of the displacement x and the velocity y and the section graphs of the joint PDFs on the surface $x = 0.485$ for different damping coefficients d_0, elastic moduli β_1, relaxation times λ_1, and restitution coefficients ρ, respectively. When $\rho = 0.95$, $\beta_1 = -0.1$, and $\lambda_1 = 0.5$ are selected, the joint PDFs decreases as $|d_0|$ increases, reflecting the effect of the reduced damping on the small displacement and velocity. In Fig. 8(c), it demonstrates the process of evolving from a unimodal shape of joint PDFs, which shows at the position of the rigid barrier, to a bimodal shape, i.e., the shape of crater in Fig. 8(b). Figures 9(a)–9(d) further provide the corresponding contours. When $d_0 = -0.015$ in Fig. 9(a), there exists one stochastic attractor, characterized by small-amplitude oscillations around the origin. And when d_0 reaches -0.035, the stochastic attractor is transformed into the characterization of large-amplitude oscillations. When d_0 is further changed to -0.045 and -0.05 in Figs. 9(c) and 9(d), the small-amplitude oscillations around the origin appear again and get stronger, while the existing large-amplitude oscillations is weakened. Clearly, it indicates that the occurrence of stochastic P-bifurcation exists in the process of variations of d_0 based upon the concept of stochastic bifurcation (phenomenological or P-bifurcations are observed when the underlying probabilistic structure of the long-term behavior of the state variables undergoes topological changes with certain parameter variations),[46–49] and it occurs when d_0 is close to -0.029, and the stability of system is changed here.

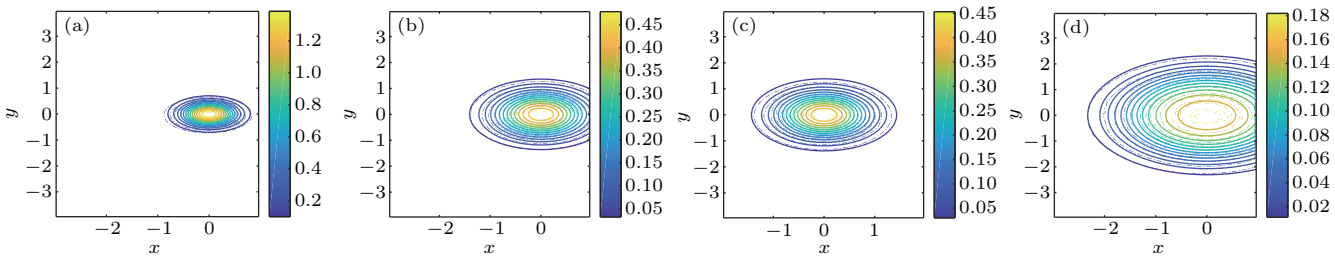


Fig. 6. The contours for joint PDFs of the displacement x and the velocity y solved both analytically (solid line) and numerically (pecked line) with different elastic modulus values β_1: (a) $\beta_1 = -0.5$, (b) $\beta_1 = -0.19$, (c) $\beta_1 = -0.19$, $S_0 = 1.985$, and (d) $\beta_1 = -0.06$.

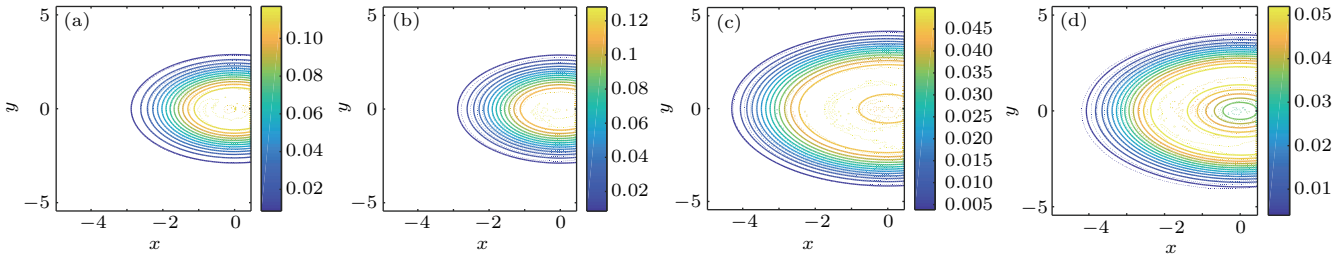


Fig. 7. The contours for joint PDFs of the displacement x and the velocity y solved both analytically (solid line) and numerically (dotted line) with different bifurcation parameters: (a) $\beta_1 = 0.0$, (b) $\lambda_1 = 0.01$, (c) $\rho = 1.0$, and (d) $d_0 = -0.05$.

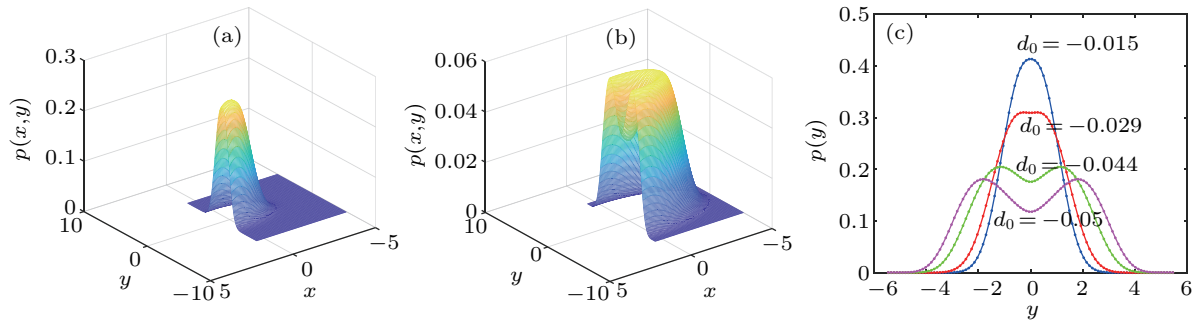


Fig. 8. The surface for joint PDFs of the displacement x and the velocity y with the damping coefficient (a) $d_0 = -0.015$ and (b) $d_0 = -0.05$; (c) the sectional views of joint PDFs on the surface $x = 0.485$ with variations of the damping coefficient d_0.

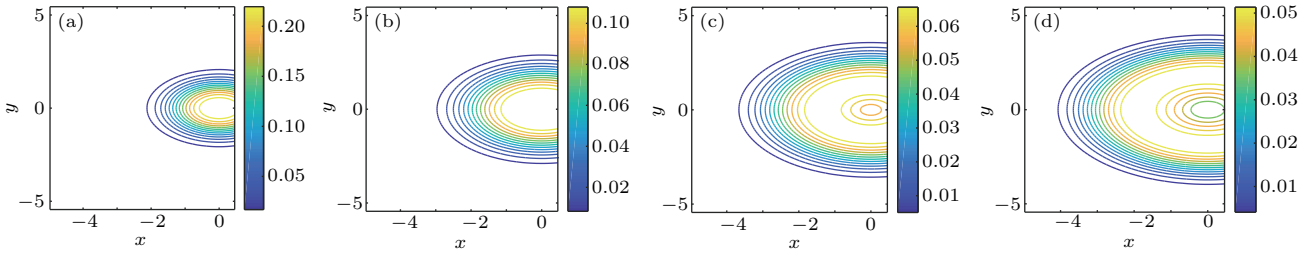


Fig. 9. Contour plots for joint PDFs of the displacement x and the velocity y: (a) $d_0 = -0.015$, (b) $d_0 = -0.035$, (c) $d_0 = -0.045$, and (d) $d_0 = -0.05$.

When d_0 returns to the initial value, a non-negative value of the elastic modulus β_1 of viscoelastic force induces a similar phenomenon. Figures 10(a) and 10(b) illustrate the joint stationary PDFs with the shape of crater for $\beta_1 = 0.0$ and $\beta_1 = 0.06$, which are different from the effect in Fig. 6. It intuitively shows the evolution process of the joint PDFs from the unimodal shape to the shape of crater caused by varying β_1 from negative to zero and then to positive (equivalent to reducing damping) through the section graphs of joint PDFs when x reaches the position of rigid barrier in Fig. 10(c). Hence, it can be seen that the stochastic P-bifurcation occurs when β_1 approximates to -0.02, which is treated as the watershed of joint PDFs from the singular peak to the shape of crater. Figures 11(a)–11(d) also report the corresponding contours. The variation of the stochastic attractor caused by varying β_1 from negative to zero and then to positive is close to the effect of the increase of $|d_0|$ in Fig. 9.

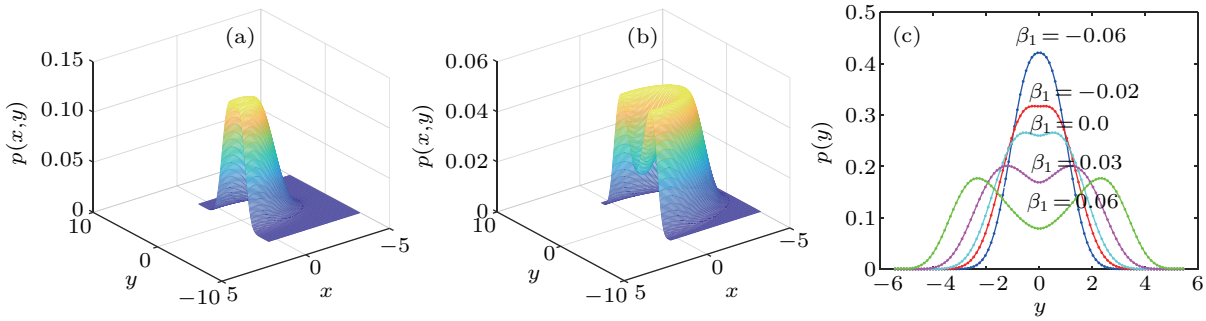


Fig. 10. The surface for joint PDFs of the displacement x and the velocity y with the elastic modulus (a) $\beta_1 = 0.0$ and (b) $\beta_1 = 0.06$; (c) the sectional views of joint PDFs on the surface $x = 0.485$ with variations of the elastic modulus β_1.

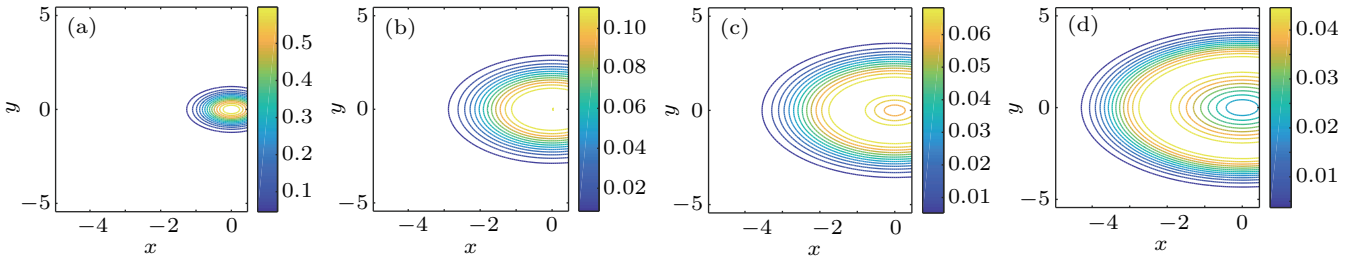


Fig. 11. Contour plots for joint PDFs of the displacement x and the velocity y: (a) $\beta_1 = -0.21$, (b) $\beta_1 = 0.0$, (c) $\beta_1 = 0.03$, and (d) $\beta_1 = 0.06$.

Further, we examine the relaxation time λ_1 of viscoelastic force from the vicinity of the usual value 1.0 to a wider range, and obtain interesting observations. Figures 12(a) and 12(b) exhibit joint stationary PDFs possessing the shape of crater for $\lambda_1 = 0.01$ and $\lambda_1 = 2.7$, which are different from the effect in Fig. 3. Figure 12(c) intuitively shows the evolution process of the joint PDFs from the unimodal shape to the shape of crater as λ_1 varies from 0.01 to 0.37 and from 1.59 to 2.7 (equivalent to reducing damping) through the section views of joint PDFs when x reaches the position of rigid barrier. Clearly, it can be seen the stochastic P-bifurcation occurs when λ_1 approximates to 0.13 or 1.87. The corresponding contours depicted in Figs. 13(a)–13(d) show that the transformation on the characterization of the stochastic attractor from small-amplitude oscillations around the origin to large-amplitude oscillations indeed exists in the above two intervals, which has not been covered before.

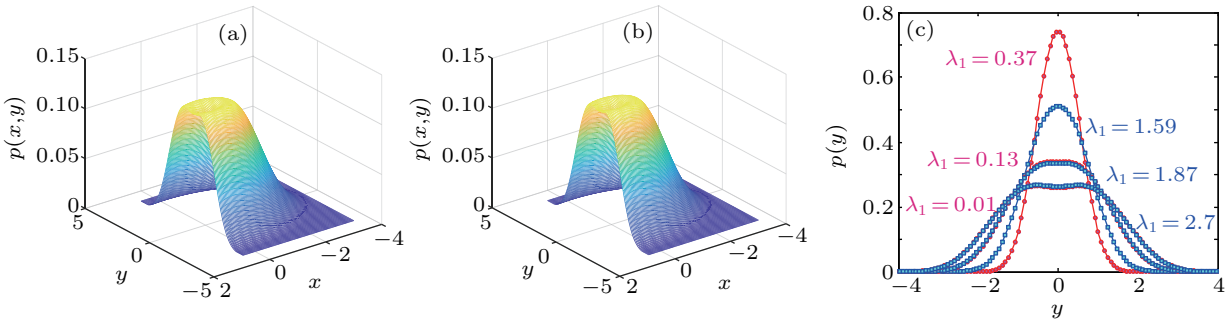


Fig. 12. The surface for joint PDFs of the displacement x and the velocity y with the relaxation time (a) $\lambda_1 = 0.01$ and (b) $\lambda_1 = 2.7$; (c) the sectional views of joint PDFs on the surface $x = 0.485$ with variations of the relaxation time λ_1.

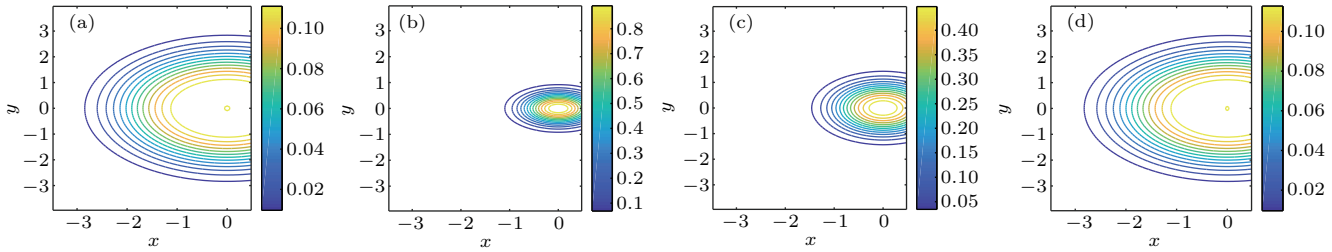


Fig. 13. Contour plots for joint PDFs of the displacement x and the velocity y: (a) $\lambda_1 = 0.01$, (b) $\lambda_1 = 0.5$, (c) $\lambda_1 = 1.5$, and (d) $\lambda_1 = 2.7$.

Then choose $\beta_1 = -0.1$ and $\lambda_1 = 0.65$, we further consider the effect of the restitution factor ρ limited to the range 0.9–1.0 on the system response. The effect of impact is to increase the damping associated with the system, and qualitatively, decreasing ρ is equivalent to increasing the damping parameter. The stationary joint PDFs are computed for the cases $\rho = 0.917$ and 1.0, as shown in Figs. 14(a) and 14(b). It decreases for the small displacement and velocity when ρ reaches 1.0, representing the classical elastic impact, and the shape of the crater also appears in the figure. The section views of joint PDFs in Fig. 14(c) further describe the evolution process caused by ρ on the surface of rigid wall and report the watershed quickly, i.e., when ρ approximates to 0.968, the stochastic P-bifurcation occurs, and it becomes double peaks when $\rho = 1.0$, corresponding to the shape of the crater in Fig. 14(b). Figures 15(a)–15(d) also provide the corresponding contour plots. The characterization of the stochastic attractors develops into large amplitude oscillations at $\rho = 0.986$ in Fig. 15(b), and both small amplitude oscillations and large amplitude oscillations are visible in Figs. 15(c) and 15(d).

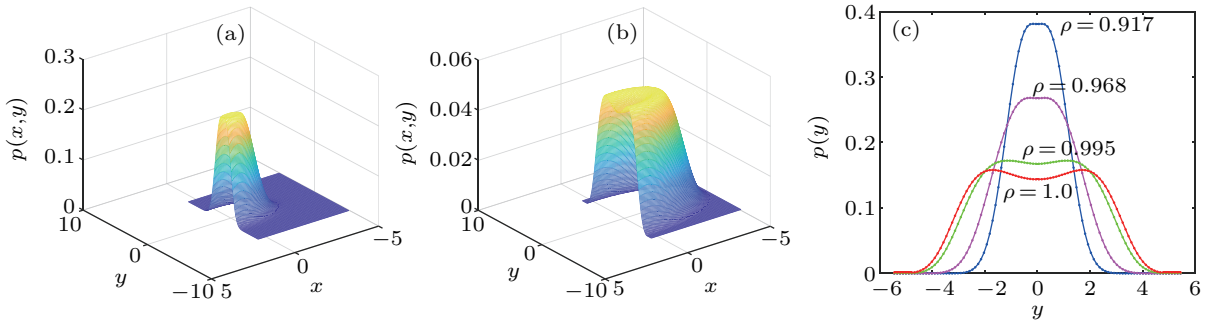


Fig. 14. The surface for joint PDFs of the displacement x and the velocity y with the restitution coefficients (a) $\rho = 0.917$ and (b) $\rho = 1.0$; (c) the sectional views of joint PDFs on the surface $x = 0.485$ with variations of the restitution coefficients ρ.

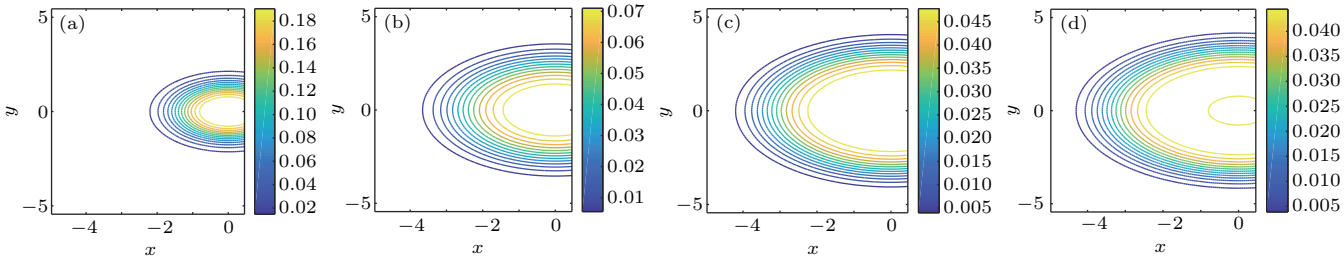


Fig. 15. Contour plots for joint PDFs of the displacement x and the velocity y: (a) $\rho = 0.917$, (b) $\rho = 0.986$, (c) $\rho = 0.9977$, and (d) $\rho = 1.0$.

5. Conclusions

In this paper, stationary responses have been exhibited to characterize the vibration law of the stochastic viscoelastic system with right nonzero offset barrier impacts. First, the viscoelastic force is replaced by a combination of equivalent effect terms. The motions of free VI systems are sorted into periodic motion without impact and quasi-periodic motion with impact based on the levels of system energy. Then, the impact condition for the displacement and velocity is transformed into the system energy description. The stationary PDFs of system are then obtained by utilizing SAEE based upon the assumption of lightly damping and weakly random perturbation, and the accuracy of the method is substantiated by comparing the theoretical results with those from MC simulations via the variations of the noise intensity, the viscoelastic parameters, the position of right nonzero rigid wall, and the restitution factor. Through the presented approach, the stochastic P-bifurcation is explored, which occurs when any of the damping coefficient, the elastic modulus, the relaxation time, or the restitution factor arrives at the watershed of joint stationary PDFs from the unimodal shape to the shape of crater, and the system stability is changed here. It is interesting that the change of elastic modulus from negative to zero and then to positive, instead of just the negative value in the previous considerations, has witnessed the evolution process of stochastic P-bifurcation. From the vicinity of the usual value to a wider range, the relaxation time induces the stochastic P-bifurcation in the two interval schemes. The suggested procedure shows some advantages, including conciseness and operability. It is a significant study for seeking the viscoelastic property and the impact condition in the future.

References

[1] Mrlík M, Ilcikova M, Sedlacik M, Mosnacek J, Peer P and Filip P 2014 *Colloid Polym. Sci.* **292** 2137
[2] Arenas J P and Crocker M J 2010 *Sound Vib.* **44** 12
[3] Lu L M, Wen J H, Zhao H G and Wen X S 2014 *Acta Phys. Sin.* **63** 154301 (in Chinese)
[4] Kiik J C, Kurasov P and Usman M 2015 *Phys. Lett. A* **379** 1871
[5] Khan Z, El Naggar M and Cascante G 2011 *J. Franklin I.* **348** 1363
[6] Findley W N and Davis F A 2013 *Creep and Relaxation of Nonlinear Viscoelastic Materials* (Amsterdam: North-Holland)
[7] Del Nobile M, Chillo S, Mentana A and Baiano A 2007 *J. Food Eng.* **78** 978
[8] Renaud F, Dion J L, Chevallier G, Tawfiq I and Lemaire R 2011 *Mech. Syst. Signal. Pr.* **25** 991
[9] Christensen R 2012 *Theory of Viscoelasticity: an Introduction* (New York: Academic Press)
[10] Roscoe R 1950 *Br. J. Appl. Phys.* **1** 171
[11] Drozdov A D 1998 *Viscoelastic Structures: Mechanics of Growth and Aging* (San Diego: Academic Press)
[12] de Espíndola J J, Bavastri C A and Lopes E M 2010 *J. Franklin I.* **347** 102
[13] Han X and Wang M 2009 *Math. Methods Appl. Sci.* **32** 346
[14] Zhu W Q 1992 *Random Vibration* (Beijing: Science Press) (in Chinese)
[15] Potapov V 1997 *J. Appl. Math. Mech.* **61** 287
[16] Zhu W Q and Cai G Q 2011 *Internat. J. Non-Linear Mech.* **46** 720
[17] Huang Q H and Xie W C 2008 *J. Appl. Mech.* **75** 021012
[18] Di Paola M, Failla G and Pirrotta A 2012 *Probabilist. Eng. Mech.* **28** 85
[19] Soize C and Poloskov I E 2012 *Comput. Math. Appl.* **64** 3594
[20] Zhu W Q 1996 *Appl. Mech. Rev.* **49** S72
[21] Brogliato B 1996 *Nonsmooth Impact Mechanics: Models, Dynamics and Control*, LNCIS 220 (Berlin: Springer Verlag)
[22] Shaw S and Holmes P 1983 *J. Appl. Mech.* **50** 849
[23] Dankowicz H and Nordmark A B 2000 *Phys. D* **136** 280
[24] Dimentberg M and Iourtchenko D 2004 *Nonlinear Dynam.* **36** 229
[25] Feng Q 2003 *Comput. Methods Appl. Mech. Eng.* **192** 2339
[26] Feng Q and He H 2003 *Eur. J. Mech. A Solids* **22** 267
[27] Namachchivaya N S and Park J H 2005 *J. Appl. Mech.* **72** 862
[28] Park J H and Namachchivaya N S 2004 *ASME 2004 International Mechanical Engineering Congress and Exposition* November 13–19, 2004 Anaheim, USA, pp. 189–200
[29] Zhuravlev V F 1976 *Mech. Solids* **11** 23
[30] Wu Y and Zhu W Q 2008 *Phys. Lett. A* **372** 623
[31] Feng J, Xu W and Wang R 2008 *J. Sound Vib.* **309** 730
[32] Dimentberg M, Gaidai O and Naess A 2009 *Internat. J. Non-Linear Mech.* **44** 791
[33] Wang D L, Xu W and Zhao X R 2016 *Chaos* **26** 033103
[34] Feng J Q, Xu W and Niu Y J 2010 *Acta Phys. Sin.* **59** 157 (in Chinese)
[35] Kumar P, Narayanan S and Gupta S 2014 *Probabilist. Eng. Mech.* **38** 143
[36] Kumar P, Narayanan S and Gupta S 2016 *Nonlinear Dynam.* **85** 439
[37] Kumar P, Narayanan S and Gupta S 2017 *Int. J. Mech. Sci.* **127** 103
[38] Su M B and Rong H W 2011 *Chin. Phys. B* **20** 060501
[39] Rong H W, Wang X D, Xu W and Fang T 2005 *Acta Phys. Sin.* **54** 4610 (in Chinese)
[40] Ma S J, Xu W and Li W 2006 *Acta Phys. Sin.* **55** 4013 (in Chinese)
[41] Yang L H, Ge Y and Ma X K 2017 *Acta Phys. Sin.* **66** 190501 (in Chinese)
[42] Li W, Zhang M T and Zhao J F 2017 *Chin. Phys. B* **26** 090501
[43] Kumar P, Narayanan S and Gupta S 2016 *Probabilist. Eng. Mech.* **45** 70
[44] Kumar P, Narayanan S and Gupta S 2016 *Procedia Eng.* **144** 998
[45] Zhu W Q and Lin Y K 1991 *J. Eng. Mech.* **117** 1890
[46] Xu W, He Q, Rong H W and Fang T 2003 *Proceedings of the Fifth International Conference on Stochastic Structural Dynamics–SSD03* (Zhu W Q Ed.) (Boca Raton: CRC Press) pp. 509–515
[47] Dtchetgnia Djeundam S, Yamapi R, Kofane T and Aziz-Alaoui M 2013 *Chaos* **23** 033125
[48] Arnold L 2013 *Random Dynamical Systems* (Berlin: Springer-Verlag)
[49] Zakharova A, Feoktistov A, Vadivasova T and Schöll E 2013 *Eur. Phys. J. Spec. TOP.* **222** 2481